

1 **Simulation of ozone-vegetation coupling and feedback in**
2 **China using multiple ozone damage schemes**

3
4
5 Jiachen Cao¹, Xu Yue^{1*}, Mingrui Ma²
6

7 1. Jiangsu Key Laboratory of Atmospheric Environment Monitoring and Pollution
8 Control, Collaborative Innovation Center of Atmospheric Environment and Equipment
9 Technology, School of Environmental Science and Engineering, Nanjing University of
10 Information Science & Technology (NUIST), Nanjing, 210044, China
11 2. State Key Laboratory of Pollution Control and Resource Reuse, School of the
12 Environment, Nanjing University, Nanjing, 210044, China

13
14
15
16 *Corresponding author: Xu Yue

17 email: yuexu@nuist.edu.cn

Abstract

As a phytotoxic pollutant, surface ozone (O_3) not only affects plant physiology but also influences meteorological fields and air quality by altering leaf stomatal functions. Previous studies revealed strong feedbacks of O_3 -vegetation coupling in China but with large uncertainties due to the applications of varied O_3 damage schemes and chemistry-vegetation models. In this study, we quantify the O_3 vegetation damage and the consequent feedbacks to surface meteorology and air quality in China by coupling two O_3 damage schemes (S2007 vs. L2013) into a fully coupled regional meteorology-chemistry model. With different schemes and damaging sensitivities, surface O_3 is predicted to decrease summertime gross primary productivity by 5.5%-21.4% and transpiration by 5.4%-23.2% in China, in which the L2013 scheme yields 2.5-4 times of losses relative to the S2007 scheme. The damages to photosynthesis of sunlit leaves are ~2.6 times that of shaded leaves in the S2007 scheme but show limited differences in the L2013 scheme. Though with large discrepancies in offline responses, the two schemes yield similar magnitude of feedback to surface meteorology and O_3 air quality. The O_3 -induced damage to transpiration increases national sensible heat by 3.2-6.0 W m^{-2} (8.9% to 16.2%) while reduces latent heat by 3.3-6.4 W m^{-2} (-5.6% to -17.4%), leading to a 0.2-0.51 °C increase in surface air temperature and a 2.2-3.9% reduction in relative humidity. Meanwhile, surface O_3 concentrations on average increase by 1.3 3.32.6-4.4 $\mu\text{g m}^{-3}$ due to the inhibitions of stomatal uptake and the anomalous enhancement in isoprene emissions, the latter of which is attributed to the surface warming by O_3 -vegetation coupling. Our results highlight the importance of O_3 control in China due to its adverse effects on ecosystem functions, deterioration of global warming, and exacerbation of O_3 pollution through the O_3 -vegetation coupling.

50 **Keywords:** Ozone, vegetation, feedback, meteorology, air quality, regional model

52 **1 Introduction**

53 Surface ozone (O_3) is one of the most enduring air pollutants affecting air quality
54 in China, with detrimental effects on human health and ecosystem functions (Monk et
55 al., 2015). Long-term observations and numerical simulations have shown that O_3
56 affects stomatal conductance (Li et al., 2017), accelerates vegetation aging (Feng et al.,
57 2015), and reduces photosynthesis (Wittig et al., 2007). These negative effects altered
58 carbon allocation (Yue and Unger, 2014; Lombardozzi et al., 2015) and inhibited plant
59 growth (Li et al., 2016), ~~leading to a decreased strength of suppressing~~ ecosystem carbon
60 uptake (Ainsworth, 2012). Moreover, these effects have profound implications for
61 global/regional climate and atmospheric environment. Given the significant ecological
62 impacts, a systematic quantification of the O_3 vegetation damage effect in China is of
63 great importance for the better understanding of the side effects of O_3 pollution on both
64 regional carbon uptake and climate change.

65 At present, field experiments on O_3 -induced vegetation damage have been
66 conducted in China but were mostly confined to individual monitoring sites. For
67 instance, Su et al. (2017) conducted experiments on grassland in Inner Mongolia and
68 found that elevated O_3 concentrations resulted in a decrease of approximately 20% in
69 the photosynthetic rate of herbaceous plants. Meta-analysis of tropical, subtropical, and
70 temperate tree species in China found that increased O_3 concentrations reduced net
71 photosynthesis and total biomass of Chinese woody plants by 28% and 14%,
72 respectively (Li et al., 2017). However, most of these experiments were conducted
73 using open-top chambers with artificially controlled O_3 concentrations, rather than
74 actual surface O_3 concentrations, making it difficult to quantitatively estimate the
75 impact of ambient O_3 on vegetation productivity. Furthermore, the spatial coverage of
76 field experiments is limited, which hinders the direct use of observational data for
77 assessing O_3 vegetation damage in different regions of China.

78 Alternatively, numerical models provide a more feasible approach to quantify the
79 O_3 -induced vegetation damage from the regional to global scales. Currently, there are
80 three main parameterizations for the calculation of ozone vegetation damage. Felzer et

81 al. (2004) established an empirical scheme based on the Accumulated Ozone exposure
82 over a Threshold of 40 ppb (AOT40) within the framework of a terrestrial ecosystem
83 model. They further estimated that O₃ pollution in the United States led to a decrease
84 in net primary productivity (NPP) by 2.6% to 6.8% during the period of 1980-1990.
85 However, the AOT40 is related to O₃ concentrations alone and ignores the biological
86 regulations on the O₃ stomatal uptake, leading to inconsistent tendencies between O₃
87 pollution level and plant damage at the drought conditions (Gong et al., 2021). In
88 acknowledge of such deficit, Sitch et al. (2007) proposed a semi-mechanistic scheme
89 calculating O₃ vegetation damage based on the stomatal uptake of O₃ fluxes and the
90 coupling between stomatal conductance and leaf photosynthesis. Yue and Unger (2014)
91 implemented this scheme into the Yale Interactive terrestrial Biosphere (YIBs) model.
92 Taking into account varied O₃ sensitivities of different vegetation types, they estimated
93 that surface O₃ led to reductions of 2-5% in the summer gross primary productivity
94 (GPP) in eastern U.S. from 1998 to 2007. Later, Lombardozzi et al. (2013) conducted
95 a meta-analysis using published chamber data and found different levels of responses
96 to O₃ exposure between stomatal conductance and photosynthesis. They further
97 implemented the independent response relationships into the Community Land Model
98 (CLM) and estimated that current ozone levels led to a reduction in global GPP by 8%-
99 12% (Lombardozzi et al., 2015).

100 The O₃ stress on vegetation physiology can feed back to affect regional climate.
101 Lombardozzi et al. (2015) employed the CLM model and found that current O₃
102 exposure reduced transpiration by 2%-2.4% globally and up to 15% regionally over
103 eastern U.S., Europe, and Southeast Asia, leading to further perturbations in surface
104 energy ~~and runoff balance~~. In U.S., Li et al. (2016) found that the O₃ vegetation damage
105 reduced latent heat (LH) flux, precipitation, and runoff by 10-27 W m⁻², 0.9-1.4 mm d⁻¹,
106 and 0.1-0.17 mm d⁻¹, respectively, ~~but and~~ increased surface air temperature by 0.6-
107 2.0 °C during the summer of 2007-2012. In China, Zhu et al. (2022) performed
108 simulations and found that the inclusion of O₃-vegetation interaction caused a 5-30 W
109 m⁻² decrease in LH, 0.2-0.8 °C increase in surface air temperature, and 3% reduction in

110 ~~relative humidity~~ during summers of 2014-2017. Recently, Jin et al.
111 (2023) applied a different regional model and estimated that O₃ exposure weakened
112 plant transpiration and altered surface heat flux in China, resulting in significant
113 increase of up to 0.16 °C in maximum daytime temperature and decrease of -0.74% in
114 relative humidity. However, all these previous estimates of O₃-induced feedback to
115 climate were derived using the empirical O₃ damage scheme proposed by Lombardozzi
116 et al. (2013), which assumed fixed damage ratios independent of O₃ dose for some
117 vegetation species and as a result may have biases in the further estimated feedback to
118 climate.

119 The O₃-vegetation coupling also has intricate implications for air quality. On one
120 hand, O₃-vegetation coupling can influence meteorological conditions that affect O₃
121 generation, ultimately influencing the O₃ level (Sadiq et al., 2017). On the other hand,
122 it can also influence biogenic emissions and dry deposition, thereby affecting O₃
123 concentrations (Gong et al., 2020). Sadiq et al. (2017) implemented O₃-vegetation
124 coupling in the Community Earth System Model (CESM) and estimated that surface
125 O₃ concentrations increased 4-6 ppb in Europe, North America, and China due to O₃-
126 vegetation coupling. By using the CLM model with the empirical scheme of
127 Lombardozzi et al. (2013), Zhou et al. (2018) found that O₃-induced damage on leaf
128 area index (LAI) could lead to changes in global O₃ concentrations by -1.8 to +3 ppb
129 in boreal summer. Gong et al., (2020) used the O₃ damage scheme from Sitch et al.
130 (2007) embedded in a global climate-chemistry-carbon coupled model and estimated
131 that O₃-induced stomatal inhibition led to an average surface O₃ increase of 1.2-2.1 ppb
132 in eastern China and 1.0-1.3 ppb in western Europe. Different from the above global
133 simulations with coarse resolutions, regional modeling with fine resolution can reveal
134 more details about O₃-vegetation coupling and feedback to surface O₃ concentrations
135 in China (Zhu et al., 2022; Jin et al., 2023). However, all these regional simulations
136 were carried out using O₃ damage scheme of Lombardozzi et al. (2013), limiting the
137 exploration of model uncertainties due to varied O₃ vegetation damage schemes.

138 In this study, we implemented O₃ vegetation damage schemes from both Sitch et

139 al. (2007) and Lombardozzi et al. (2013) into the widely-used regional meteorology-
140 chemistry model WRF-Chem. We validated the simulated meteorology and O₃
141 concentrations, and performed sensitivity experiments to explore the O₃ damage to GPP
142 and consequent feedbacks to regional climate and air quality in China. Within the same
143 framework, we compared the differences of O₃-vegetation coupling from two schemes
144 and explored the causes for the discrepancies. We aimed to quantify the modeling
145 uncertainties in the up-to-date estimates of O₃ impact on regional carbon fluxes and its
146 feedback to regional climate and air quality in China.

147

148 **2 Method**

149 **2.1 WRF-Chem model**

150 We used WRF-Chem model version 3.9.1 to simulate meteorological fields and
151 O₃ concentration in China. The model includes atmospheric physics and dynamical
152 processes, atmospheric chemistry, and biophysical and biochemical processes (Grell et
153 al., 2005, Skamarock et al., 2008). The model domain is configured with 196×160 grid
154 cells at 27 km horizontal resolution on the Lambert conformal projection, and covers
155 the entire mainland China. In the vertical direction, 28 layers are set extending from
156 surface to 50 hPa. The meteorological initial and boundary conditions were adopted
157 from ERA5 reanalysis produced by the European Centre for Medium-Range Weather
158 Forecasts (ECMWF) at a horizontal resolution of 0.25°×0.25° (Hersbach et al., 2020).
159 The chemical initial and boundary conditions were generated from the Model for Ozone
160 and Related Chemical Tracer version 4 (MOZART-4), which is available at a horizontal
161 resolution of 1.9°×2.5° with 56 vertical layers (Emmons et al., 2010).

162 Anthropogenic emissions are adopted from the 0.25° Multi-resolution Emission
163 Inventory for China (MEIC) and MIX Asian emission inventory for the other regions
164 (available at <http://meicmodel.org>). Biogenic emissions are calculated online using the
165 Model of Emissions of Gases and Aerosols from Nature (Guenther et al., 2006), which
166 considers the impacts of plant types, weather conditions, and leaf area on vegetation
167 emissions. Atmospheric chemistry is simulated using the Carbon Bond Mechanism

168 version Z (CBMZ) (Zaveri and Peters, 1999) gas-phase chemistry module coupled with
169 a four-bin sectional Model for Simulating Aerosol Interactions and Chemistry
170 (MOSAIC) (Zaveri et al., 2008). The photolysis scheme is based on the Madronich
171 Fast-TUV photolysis module (Tie et al., 2003). The physical configurations include the
172 Morrison double-moment microphysics scheme (Morrison et al., 2009), the Grell-3
173 cumulus scheme (Grell et al., 2002), the Rapid Radiative Transfer Model longwave
174 radiation scheme (Mlawer et al., 1997), the Goddard short-wave radiation scheme
175 (Chou and Suarez, 1994), the Yonsei University planetary boundary layer scheme
176 (Hong et al., 2006), and the revised MM5 (Fifth generation Mesoscale Model) Monin–
177 Obukhov surface layer scheme.

178

179 **2.2 Noah-MP model**

180 Noah-MP is a land surface model coupled to WRF-Chem with multiple options
181 for key land-atmosphere interaction processes (Niu et al., 2011). Noah-MP considers
182 canopy structure with canopy height and crown radius, and depicts leaves with
183 prescribed dimensions, orientation, density, and radiometric properties. The model
184 employs a two-stream radiative transfer approach for surface energy and water transfer
185 processes (Dickinson, 1983). Noah-MP is capable of distinguishing photosynthesis
186 pathways between C₃ and C₄ plants, and defines vegetation-specific parameters for leaf
187 photosynthesis and respiration.

188 Noah-MP considers prognostic vegetation growth through the coupling between
189 photosynthesis and stomatal conductance (Farquhar et al., 1980; Ball et al., 1987). The
190 photosynthesis rate, A ($\mu\text{molCO}_2 \text{ m}^{-2} \text{ s}^{-1}$), is calculated as one of three limiting factors
191 as follows:

$$192 A_{tot} = \min (W_c, W_j, W_e) I_{gs} \quad (1)$$

193 where W_c is the RuBisCO-limited photosynthesis rate, W_j is the light-limited
194 photosynthesis rate, and W_e is the export-limited photosynthesis rate. I_{gs} is the
195 growing season index with values ranging from 0 to 1. Stomatal conductance (g_s) is
196 computed based on photosynthetic rate as follows:

197
$$g_s = \frac{1}{r_s} = m \frac{A_{net}}{C_s} RH + b \quad (2)$$

198 where b is the minimum stomatal conductance; m is the Ball-Berry slope of the
 199 conductance-photosynthesis relationship; A_{net} is the net photosynthesis by subtracting
 200 dark respiration from A_{tot} ; C_s is the ambient CO₂ concentration at the leaf surface. The
 201 assimilated carbon is allocated to various parts of vegetation (leaf, stem, wood, and root)
 202 and soil carbon pools (fast and slow), which determines the variations of LAI and
 203 canopy height. Plant transpiration rate is then estimated using the dynamic LAI and
 204 stomatal conductance. Noah-MP also distinguishes the photosynthesis of sunlit and
 205 shaded leaves. Sunlit leaves are more limited by CO₂ concentration while shaded leaves
 206 are more constrained by insolation, leading to varied responses to O₃ damage.

207

208 **2.3 Scheme for ozone damage on vegetation**

209 We implemented the O₃ vegetation damage schemes proposed by Sitch et al. (2007)
 210 (hereafter S2007) and Lombardozzi et al. (2013) (hereafter L2013) into the Noah-MP.
 211 In S2007 scheme, the undamaged fraction F for net photosynthesis is dependent on the
 212 sensitivity parameter a_{PFT} and excessive area-based stomatal O₃ flux, which is
 213 calculated as the difference between f_{O_3} and threshold y_{PFT} :

214
$$F = 1 - a_{PFT} \times \max\{f_{O_3} - y_{PFT}, 0\} \quad (3)$$

215 where a_{PFT} and y_{PFT} are specifically determined for individual plant functional types
 216 (PFTs) based on measurements (Table 1). The stomatal O₃ flux f_{O_3} is calculated as

217
$$f_{O_3} = \frac{[O_3]}{r_a + k_{O_3} \cdot r_s} \quad (4)$$

218 where [O₃] is the O₃ concentration at the reference level (nmol m⁻³), r_a is the
 219 aerodynamic and boundary layer resistance between leaf surface and reference level (s
 220 m⁻¹). $k_{O_3} = 1.67$ represents the ratio of leaf resistance for O₃ to that for water vapor. r_s
 221 represents stomatal resistance (s m⁻¹). For S2007 scheme, stomatal conductance is
 222 damaged with the same ratio (1- F) as photosynthesis and further affects O₃ uptake. In
 223 Noah-MP, the f_{O_3} are calculated separately for sunlit and shaded leaves with
 224 corresponding stomatal resistance (Supplementary Text S1).

225 As a comparison, the L2013 scheme applies separate O₃ damaging relationships
226 for photosynthetic rate and stomatal conductance. These independent relationships
227 account for different plant groups and are calculated based on the cumulative uptake of
228 O₃ (CUO) under different levels of chronic O₃ exposure. The leaf-level CUO (mmol m⁻
229²) over the growing season is calculated as follows:

$$230 \quad \text{CUO} = \sum(k_{O_3}/r_s + 1/r_a) \times [O_3] \quad \text{CUO} = \sum(k_{O_3}/r_s + 1/r_a) \times [O_3]$$

231 (5)

232 The physical parameters in Equation (5) are the same as those in Equation (4). O₃ uptake
233 is accumulated over time steps during the growing season with mean LAI > 0.5
234 (Lombardozzi et al., 2012), when vegetation is most vulnerable to air pollution episodes.
235 O₃ uptake is only accumulated when O₃ flux is above an instantaneous threshold of 0.8
236 nmol O₃ m⁻² s⁻¹ to account for ozone detoxification by vegetation at low O₃ levels
237 (Lombardozzi et al., 2015). We also include a leaf-turnover rate for evergreen plants so
238 that the accumulation of O₃ flux does not last beyond the average foliar lifetime. The
239 O₃ damaging ratios depend on CUO with empirical linear relationships as follows:

$$240 \quad F_{pO_3} = a_p \times CUO + b_p \quad (6)$$

$$242 \quad F_{cO_3} = a_c \times CUO + b_c \quad (7)$$

243 where F_{pO_3} and F_{cO_3} are the ozone damage ratios for photosynthesis and stomatal
244 conductance, respectively. The slopes (a_p for photosynthesis and a_c for stomatal
245 conductance) and intercepts (b_p for photosynthesis and b_c for stomatal conductance) of
246 regression functions are determined based on the meta-analysis of hundreds of
247 measurements (Table 2). The ratios predicted in Equations (6) and (7) are applied to
248 photosynthesis and stomatal conductance, respectively, to account for their independent
249 responses to O₃ damages. In Noah-MP, the F_{pO_3} and F_{cO_3} are calculated separately for
250 sunlit and shaded leaves based on corresponding stomatal resistance (Supplementary
251 Text S1).

253

254 **2.4 Observational data**

255 We validated the simulated meteorology and air pollutants with observations. The
256 meteorological data were downloaded from the National Meteorological Information
257 Center of China Meteorological Administration (CMA Meteorological Data Centre,
258 2022, <http://data.cma.cn/data/detail/dataCode/A.0012.0001.html>). The daily averaged
259 surface pressure (PRES), wind speed at a height of 10 m (WS10), relative humidity
260 (RH) and temperature at a height of 2 m (T2) were collected from 839 ground stations.
261 Hourly surface O₃ concentrations at 1597 sites in China were collected from Chinese
262 National Environmental Monitoring Center (CNEMC,
263 <http://websearch.mep.gov.cn/><http://websearch.mep.gov.cn/>).

264

265 **2.5. Simulations**

266 We performed seven experiments to quantify the damaging effects of ambient O₃
267 on GPP and the feedbacks to regional climate and air quality (Table 3). All simulations
268 are conducted from 1st May to 31st August of 2017 with the first month excluded from
269 the analysis as the spin-up. The control simulations (CTRL) excluded the impact of
270 ozone on vegetation. Three offline simulations were performed with the same settings
271 as the CTRL run, except that O₃ vegetation damages were calculated and output without
272 feedback to affect vegetation growth. These offline runs were established using either
273 the S2007 scheme (Offline_SH07 for high sensitivity and Offline_SL07 for low
274 sensitivity) or the L2013 scheme (Offline_L13). As a comparison, three online
275 simulations applied the S2007 scheme (Online_SH07 for high sensitivity and
276 Online_SL07 for low sensitivity) and the L2013 scheme (Online_L13) to estimate the
277 O₃ damages to GPP, which further influenced LAI development, leaf transpiration, and
278 dry deposition. The differences between CTRL and Online runs indicated the responses
279 of surface meteorology and O₃ concentrations to the O₃-induced vegetation damages.

280

281 **3. Results**

282 **3.1 Model evaluations**

283 We compared the simulated summer near-surface temperature, relative humidity,

wind speed, and surface O₃ concentrations to observations. The model reasonably reproduces the spatial pattern of higher near-surface temperature with warmings in the Southeast and Northwest but coolings and lower temperature over the Tibetan Plateau (Figure 1a). On the national scale, the near-surface temperature is underestimated with a mean bias (MB) of 1.04 °C and but it shows a spatial high correlation (R-of=0.96-). Unlike temperature, simulated relative humidity is overestimated with a MB of 5.04 % but a high R of 0.93 (Figure 1b). Due to the modeling biases in the topographic effects, simulated wind speed is overestimated by more than 1.06 m s⁻¹ on the national scale (Figure 1c). Such overestimation was also reported in other studies using WRF models (Hu et al., 2016, Liu et al., 2020, Zhu et al., 2022).

Comparisons with the measurements from air quality sites show that the simulated O₃ deviates from the observed mean concentrations by 5.42 μg m⁻³ with a spatial R of 0.68. The model reasonably captures the hotspots over North China Plain though with some overestimations, potentially attributed to uncertain emissions and coarse model resolutions. Such elevated bias in summer O₃ is a common issue for both global and regional models over Asia. For example, Zhu et al. (2022) reported the overestimated summer average ozone concentration by 13.82 μg m⁻³ in China. Liu et al. (2020) reached positive biases ranging from 3.7 μg m⁻³ to 13.32 μg m⁻³ using the WRF-CMAQ model. Overall, the WRF-Chem model shows reasonable performance in the simulation of surface meteorology and O₃ concentrations in China.

304

305 **3.2 Offline O₃ damage**

306 We compared the offline O₃ damage to photosynthesis between sunlit (PSNSUN) 307 and shaded (PSNSHA) leaves during the summer. The S2007 scheme is dependent on 308 instantaneous O₃ uptake, which peaks when both O₃ concentrations and stomatal 309 conductance are high. For the same O₃ pollution level, the damages are much higher 310 for the sunlit leaves (Figures 2a-2b) than that for the shaded leaves (Figures 2d-2e), 311 because of the higher stomatal conductance linked with the more active photosynthesis 312 for the sunlit leaves. In contrast, the L2013 scheme depends on the accumulated O₃ flux,

313 which results and assumes constant damages for some PFTs (Table 2), resulting in
314 vegetation damage reductions of photosynthesis even at lower instant low O₃
315 concentrations. As a result Consequently, we found limited differences in the O₃
316 damages between sunlit (Figure 2c) and shaded (Figure 2f) leaves with L2013 scheme.
317 Observations have reported that surface O₃ has limited impacts on the shaded leaves
318 (Wan et al., 2014), consistent with the results simulated by the S2007 scheme.
319 Furthermore, surface O₃ concentrations are low in southwest during summer (Figure
320 1d), suggesting a low O₃ vegetation damage over Tibetan Plateau and the more
321 reasonable performance with the S2007 scheme.

322 Figure 3 shows the effect of O₃ damage to stomatal resistance of sunlit (RSSUN)
323 and shaded (RSSHA) leaves. Overall, the spatial pattern of the changes in stomatal
324 resistance is consistent with those of photosynthesis (Figure 2) but with opposite signs.
325 Both RSSUN and RSSHA are enhanced by O₃ damage so as to prevent more O₃ uptake.
326 For S2007 scheme, RSSUN with high and low sensitivities respectively increases by
327 13.43% (Figure 3a) and 8.35% (Figure 3b), higher than the rates of 4.71% (Figure 3d)
328 and 2.97% (Figure 3e) for RSSHA. These ratios are inversely connected to the changes
329 of photosynthesis (Figure 2), suggesting the full coupling of damages between leaf
330 photosynthesis and stomatal conductance. For L2013 scheme, predicted changes in
331 RSSUN (Figure 3c) and RSSHA (Figure 3f) are very similar with the magnitude of
332 25.3%-26.3%. These changes are higher than the loss of photosynthesis (Figures 2c and
333 2f), suggesting the decoupling of O₃ damages to leaf photosynthesis and stomatal
334 conductance as revealed by the L2013 scheme.

335 We further assessed the O₃ damage to GPP and transpiration (TR). For S2007
336 scheme, O₃ causes damages to national average GPP and TR approximately by 5.5%
337 with low sensitivity (Figures 4b and 4e) and 8.4% with high sensitivity (Figures 4a and
338 4d) compared to the CTRL simulation. The model predicts high GPP damages over
339 North China Plain and moderate damages in the southeastern and northeastern regions.
340 In the northwest, GPP damage is very limited due to the low relative humidity (Figure
341 1b) that constrains the stomatal uptake. For L2013 scheme, TR shows uniform

342 reductions exceeding -25% in most regions of China except for the northwest (Figure
343 4f), though O₃ concentrations show distinct spatial gradient (Figure 1d). The changes
344 of GPP are similar to that of TR but with lower inhibitions (Figure 4c). On average, the
345 GPP reduction with the L2013 scheme is 2.5-3.9 times of that predicted with the S2007
346 scheme. The most significant differences are located in Tibetan Plateau with limited
347 damages in S2007 but strong inhibitions of both GPP and TR in L2013. Given the cold
348 environmentThe low temperature (Figure 1a) that constrainsand O₃ concentrations
349 (Figure 1d) jointly constrain O₃ stomatal uptake (Wilkinson et al., 2001), we consider
350 theFigure S2), leading to low O₃ impacts indamages over Tibetan Plateau predicted
351 with theS2007 schemeare more reasonable. However, theL2013 schemeapplies
352 $b_p=0.8021$ for grassland (Table 2), suggesting strong baseline damages up to 20% even
353 with CUO=0 over Tibetan Plateau where the grassland dominates (Figure S3).

354

355 3.3 The O₃-vegetation feedback to surface energy and meteorology

356 The O₃ vegetation damage causes contrasting responses in surface sensible heat
357 (SH) and LH (Figure 5). For S2007 scheme, the SH fluxes on average increase by 3.17
358 W m⁻² (8.85%) with low sensitivity (Figure 5b) and 5.99 W m⁻² (16.22%) with high
359 sensitivity (Figure 5a). The maximum enhancement is located in southern China, where
360 the increased stomatal resistance (Figure 3a) reduces transpiration and the consequent
361 heat dissipation. Meanwhile, LH fluxes decrease by 3.26 W m⁻² (5.58%) with low
362 sensitivity (Figure 5e) and 6.43 W m⁻² (15.29%) with high sensitivity (Figure 5d),
363 following the reductions in transpiration (Figures 4d and 4e). We found similar changes
364 in surface energy by O₃-vegetation coupling between the S2007 and L2013 schemes.
365 The SH shows the same hotspots over southern China with national average increase
366 of 12.85% (Figure 5c), which is within the range of 8.85% to 16.22% predicted by the
367 S2007 scheme. The LH largely decreases in central and northern China with the mean
368 reduction of 17.4% (Figure 5f), close to the magnitude of 15.29% predicted with the
369 S2007 scheme using the high O₃ sensitivity (Figure 5d). Although the offline damages
370 to GPP and TR are much larger with the L2013 than S2007 (Figure 4), their feedback

371 to surface energy shows consistent spatial pattern and magnitude (Figure 5), likely
372 because the O₃ inhibition in S2007 has the same diurnal cycle with energy fluxes while
373 the L2013 scheme shows almost constant inhibitions ~~through the day (Figure S1)~~.
374 ~~The throughout the day (Figure S1). The zero or near-zero slope parameters (a_p and a_c)~~
375 ~~in the L2013 scheme (Table 2) lead to insensitive responses of photosynthesis and~~
376 ~~stomatal conductance to the variations of CUO. As a result, there were very limited~~
377 ~~diurnal variations in O₃ damage with the L2013 scheme. However, the strong nighttime~~
378 damages in L2013 have limited contributions to the changes of surface energy, which
379 usually peaks at the daytime.

380 The O₃-induced damages to stomatal conductance weaken plant transpiration and
381 thus slow down the heat dissipation at the surface, leading to the higher temperature but
382 lower RH in China (Figure 6). On the national scale, temperature increases by 0.5 °C
383 due to O₃ vegetation damage with the high sensitivity (Figure 6a) and 0.23 °C with the
384 low sensitivity (Figure 6b) predicted using the S2007 scheme. A similar warming is
385 predicted with the L2013 scheme except that temperature shows moderate enhancement
386 over Tibetan Plateau (Figure 6c). The average RH decreases by 3.68% with the high O₃
387 sensitivity (Figure 6d) and 2.22% with the low sensitivity (Figure 6e) in response to the
388 suppressed plant transpiration. A stronger RH reduction of -3.85% is achieved with the
389 L2013 scheme, which predicts the maximum RH reductions in the North (Figure 6f).
390

391 **3.4 The O₃-vegetation feedback to air quality**

392 The O₃-induced inhibition on stomatal resistance leads to a significant increase in
393 surface O₃ concentrations, particularly in eastern China (Figures 7a-7c). The main cause
394 of such feedback is the reduction in O₃ dry deposition, which exacerbates the O₃
395 pollution in China. For S2007 scheme, this positive feedback can reach up to 15 $\mu\text{g m}^{-3}$
396 with high sensitivity (Figure 7a) and 8 $\mu\text{g m}^{-3}$ with low sensitivity (Figure 7b) over
397 North China Plain. On the national scale, surface O₃ enhances ~~3.314.40~~ $\mu\text{g m}^{-3}$ (~~4.25 μg~~
398 ~~m^{-3}~~) or ~~7.925.08 %~~ with high O₃ sensitivity and ~~2.62~~ $\mu\text{g m}^{-3}$ (3.04%) with ~~low O₃~~
399 ~~sensitivity through the high (low) O₃-sensitivity coupling to vegetation~~. For L2013

400 scheme, the changes of O₃ concentration (Figure 7c) are comparable to that of the
401 S2007 scheme with high sensitivity (Figure 7a), except that the O₃ enhancement is
402 stronger in the Southeast but weaker in the Northeast.

403 The O₃-vegetation coupling also increases surface isoprene emissions. For S2007
404 scheme, isoprene emissions increase by 6.13% with high sensitivity (Figure 7d) and
405 3.43% with low sensitivity (Figure 7e), with regional hotspots in North China Plain,
406 northeastern and southern regions. The predictions using L2013 scheme (Figure 7f)
407 show very similar patterns and magnitude of isoprene changes to the S2007 scheme
408 with high sensitivity. Such enhancement in isoprene emissions is related to the
409 additional surface warming by O₃-vegetation interactions (Figures 6a-6c). In turn, the
410 increased isoprene emissions contribute to the deterioration of O₃ pollution in China.

411

412 **4. Conclusions and discussion**

413 In this study, we explored the feedback of O₃-vegetation coupling to surface
414 meteorology and air quality in China using two O₃ damage schemes embedded in a
415 regional meteorology-chemistry coupled model. The two schemes predicted distinct
416 spatial patterns with much larger magnitude of GPP loss in the L2013 scheme than that
417 in the S2007 scheme. We further distinguished the leaf responses with different
418 illuminations. For the S2007 scheme, the damages to photosynthesis of sunlit leaves
419 are ~2.6 times of that to shaded leaves. However, for the L2013 scheme, limited
420 differences are found between the sunlit and shaded leaves. The damages to leaf
421 photosynthesis increase stomatal resistance, leading to the reductions of transpiration
422 but enhancement of sensible heat due to the less efficient heat dissipation. These
423 changes in surface energy and water fluxes feed back to increase surface temperature
424 but decrease relative humidity. Although the L2013 scheme predicts much stronger
425 offline damages, the feedback causes very similar pattern and magnitude in surface
426 warming as the S2007 scheme. Consequently, surface O₃ increases due to the stomatal
427 closure and isoprene emissions enhance due to the anomalous warming.

428 Our predicted O₃ damage to GPP was within the range of -4% to -40% as estimated

429 in previous studies using different models and/or parameterizations over China (Ren et
430 al., 2011; Lombardozzi et al., 2015; Yue et al., 2015; Sadiq et al., 2017; Xie et al., 2019;
431 Zhu et al., 2022; Jin et al., 2023). Such a wide span revealed the large uncertainties in
432 the estimate of O₃ impacts on ecosystem functions. In this study, we employed two
433 schemes and compared their differences. With the S2007 scheme, we predicted GPP
434 reductions of -5.5% to -8.5% in China, This is similar to the range of -4% to -10%
435 estimated by Yue et al. (2015) using the same O₃ damage scheme ~~but~~. However, it is
436 lower than the estimate of -12.1% predicted by Xie et al. (2019), likely due to the slight
437 overestimation of surface O₃ in the latter study. With the L2013 scheme, we predicted
438 much larger GPP reductions of -21.4%. However, such value was still lower than the -
439 28.9% in Jin et al. (2023) and -20% to -40% in Zhu et al. (2022) using the same L2013
440 scheme embedded in WRF-Chem model, though all studies showed similar spatial
441 patterns in the GPP reductions. Such differences were likely attributed to the varied
442 model configuration as we ran the model from May while the other studies started from
443 the beginning of years. The longer time for the accumulation of O₃ stomatal uptake in
444 other studies ~~resulted~~might result in higher damages than our estimates with the L2013
445 scheme.

446 The O₃-vegetation coupling caused strong feedback to surface meteorology and
447 air quality. Our simulations with either scheme revealed that surface SH increases by
448 2-28 W m⁻² and LH decreases by 4-32W m⁻² over eastern China, consistent with the
449 estimates of 5-30 W m⁻² by Zhu et al. (2022) using WRF-Chem model with the L2013
450 scheme. Consequently, surface air temperature on average increases by 0.23-0.51°C
451 while relative humidity decreases by 2.2-3.8%, similar to the warming of 0.2-0.8°C and
452 RH reduction of 3% as predicted by Zhu et al. (2022). However, these changes in
453 surface energy flux and meteorology are much higher than that in Jin et al. (2023),
454 likely because the latter focuses on the perturbations averaged throughout the year
455 instead of summer period as in this study and Zhu et al. (2022). We further predicted
456 that O₃ vegetation damage increased surface O₃ by ~~0.6-1.7 ppbv~~0-3.33 $\mu\text{g m}^{-3}$ in China,
457 similar to the ~~4.2-2.1 ppbv~~3.5-4.11 $\mu\text{g m}^{-3}$ estimated for eastern China using a global

458 model (Gong et al., 2020). Regionally, the O₃ enhancement reached as high as 4-7.5
459 ppbv 84-14.70 $\mu\text{g m}^{-3}$ in North China Plain, consistent with the maximum value of 6
460 ppbv 11.76 $\mu\text{g m}^{-3}$ over the same domain predicted by Zhu et al. (2022). However,
461 limited feedback to surface O₃ was predicted in Jin et al. (2023), mainly because the
462 decreased dry deposition had comparable but opposite effects to the decreased isoprene
463 emissions due to the reductions of LAI. Such discrepancy was likely caused by the
464 stronger O₃ inhibition in Jin et al. (2023) following the longer period of O₃
465 accumulation, consequently exacerbating the negative impacts of LAI reductions on O₃
466 production.

467 There were some limitations in our parameterizations and simulations. TheFirst,
468 we predicted increases of isoprene emissions in eastern China mainly due to the
469 increased leaf temperature, which is in line with previous studies (Sadiq et al., 2017;
470 Zhu et al., 2022). However, isoprene production is coupled to photosynthesis. There are
471 empirical evidences showing that high dose of O₃ exposure reduces isoprene emissions
472 when O₃ exposure is prolonged enough to suppress photosynthesis (Bellucci et al.,
473 2023). Inclusion of such negative feedback might alleviate the O₃-induced
474 enhancement in isoprene emissions. Second, the WRF-Chem model slightly
475 overestimated summer O₃ concentrations, which could exacerbate the damages to
476 stomatal conductance and the subsequent feedback. TheThird, the S2007 scheme
477 employed the coupled responses in photosynthesis and stomatal conductance to O₃
478 vegetation damage. However, some observations revealed that stomatal response is
479 slow under long-term O₃ exposure, resulting in loss of stomatal function and decoupling
480 from photosynthesis (Calatayud et al., 2007; Lombardozzi et al., 2012). The L2013
481 scheme considered the decoupling between photosynthesis and stomatal conductance.
482 However, this scheme ~~could not distinguish the responses of shows no significant~~
483 different changes for sunlit and shaded leaves. In addition, the calculation of CUO
484 heavily relied on the ~~ezone~~O₃ threshold and accumulation period, leading to varied
485 responses among different studies using the same scheme. Furthermore, the slopes of
486 O₃ sensitivity in L2013 scheme were set to zero for some PFTs, leading to constant

487 damages independent of CUO. ~~FinallyFourth~~, the current knowledge of the O₃ effects
488 on stomatal conductance was primarily derived from leaf-level measurements
489 (Matyssek et al., 2008), which were much fewer compared to that for photosynthesis.
490 The limited data availability and lack of inter-PFT responses constrain the development
491 of empirical parameterizations.

492 Despite these limitations, our study provided the first comparison of different
493 parameterizations in simulating O₃-vegetation interactions. We found similar feedbacks
494 to surface energy and meteorology though the two schemes showed varied magnitude
495 and distribution in the offline responses of GPP and stomatal conductance to surface
496 O₃. The main cause of such inconsistency lied in the low feedback of damages in L2013
497 with some unrealistic inhibitions of ecosystem functions at night and over the regions
498 with low O₃ level. Such similarity provides a solid foundation for the exploration of
499 O₃-vegetation coupling using different schemes. The positive feedback of O₃ vegetation
500 damage to surface air temperature and O₃ concentrations posed emerging but ignored
501 threats to both climate change and air quality in China.

502

503 **Data availability**

504 ~~The observed hourly O₃ concentrations were obtained from Chinese National~~
505 ~~Environmental Monitoring Center (CNEMC, <http://websearch.mep.gov.cn/>).~~ The
506 ~~observed meteorological data were obtained from the National Meteorological~~
507 ~~Information Center of China Meteorological Administration (CMA Meteorological~~
508 ~~Data~~ ~~Centre,~~ ~~2022,~~
509 <http://data.cma.cn/data/detail/dataCode/A.0012.0001.html>[.http://data.cma.cn/data/detail/dataCode/A.0012.0001.html](http://data.cma.cn/data/detail/dataCode/A.0012.0001.html)
510 ~~. The MEIC and MIX emission inventory are available~~
511 ~~at (http://meicmodel.org.cn/?page_id=560 and http://meicmodel.org.cn/?page_id=89).~~
512 http://meicmodel.org.cn/?page_id=89.

513

514 **Author contributions**

515 ~~XY conceived the study. XY and JC designed the research and carried out the~~

516 simulations. JC completed data analysis and the first draft. MM provided useful
517 comments on the paper. XY reviewed and edited the manuscript.

518

519 **Competing interests.** The authors declare that they have no conflict of interest.

520

521 **Acknowledgements.** The authors declare are grateful to three anonymous reviewers for
522 their constructive comments that they have no conflict of interest improved this study.

523

524 **Acknowledgments**

525 **Financial support.** This study was jointly funded by the National Key Research and
526 Development Program of China (grant no. 2023YFF0805403), National Natural
527 Science Foundation of China (grant no. 42293323), and Jiangsu Funding Program for
528 Excellent Postdoctoral Talent (grant no. 2023ZB737).

529

530 **References**

531 Ainsworth, E. A., Yendrek, C. R., Sitch, S., Collins, W. J., and Emberson, L. D.: The
532 effects of tropospheric ozone on net primary productivity and implications for
533 climate change, Annu. Rev. Plant Biol., 63, 637–661,
534 <https://doi.org/10.1146/annurevplant-042110-103829>, 2012.

535 Ball, J. T., Woodrow, I. E., and Berry, J. A.: A model predicting stomatal conductance
536 and its contribution to the control of photosynthesis under different environmental
537 conditions, Prog. Photosynthesis, Springer, Dordrecht, 4, 221–224, 1987.

538 Bellucci, M., Locato, V., Sharkey, T. D., Gara D. and Loreto, F.: Isoprene emission by
539 plants in polluted environments, J. PLANT INTERACT., 18:1, 2266463,
540 <https://doi.org/10.1080/17429145.2023.2266463>, 2023

541 Calatayud, V., Cerveró, J., and Sanz, M. J.: Foliar, physiologial and growth responses
542 of four maple species exposed to ozone, Water Air Soil Pollut., 185, 239–254,
543 <https://doi.org/10.1007/s11270-007-9446-5>, 2007.

544 Chou, M.-D. and Suarez, M.J.: An Efficient Thermal Infrared Radiation
545 Parameterization for Use in General Circulation Models. Technical Report, 85p.

546 1994.

547 Dickinson, R. E.: Land surface processes and climate – Surface albedos and energy
548 balance, *Adv. Geophys.*, 25, 305–353, [https://doi.org/10.1016/S0065-2687\(08\)60176-4](https://doi.org/10.1016/S0065-2687(08)60176-4), 1983.

550 Emmons, L. K., Walters, S., Hess, P. G., Lamarque, J.-F., Pfister, G. G., Fillmore, D.,
551 Granier, C., Guenther, A., Kinnison, D., Laepple, T., Orlando, J., Tie, X., Tyndall,
552 G., Wiedinmyer, C., Baughcum, S. L., and Kloster, S.: Description and evaluation
553 of the Model for Ozone and Related chemical Tracers, version 4 (MOZART-4),
554 *Geosci. Model Dev.*, 3, 43–67, <https://doi.org/10.5194/gmd-3-43-2010>, 2010.

555 Farquhar, G. D., Caemmerer, S. V., and Berry, J. A.: A biochemicalmodel of
556 photosynthetic CO₂ assimilation in leaves of C3 species, *Planta*, 149, 78–90,
557 <https://doi.org/10.1007/bf00386231>, 1980.

558 Felzer, B., Kicklighter, D., Melillo, J., Wang, C., Zhuang, Q., and Prinn, R.: Effects of
559 ozone on net primary production and carbon sequestration in the conterminous
560 United States using a biogeochemistry model, *Tellus B*, 56, 230–248,
561 <https://doi.org/10.1111/j.1600-0889.2004.00097.x>, 2004.

562 Feng, Z., Hu, E., Wang, X., Jiang, L., and Liu, X.: Ground-level O₃ pollution and its
563 impacts on food crops in China: A review, *Environ. Pollut.*, 199, 42–48,
564 <https://doi.org/10.1016/j.envpol.2015.01.016>, 2015.

565 Gong, C., Lei, Y., Ma, Y., Yue, X., and Liao, H.: Ozone– vegetation feedback through
566 dry deposition and isoprene emissions in a global chemistry–carbon–climate
567 model, *Atmos. Chem. Phys.*, 20, 3841–3857, <https://doi.org/10.5194/acp-203841-2020>, 2020.

569 Gong, C., Yue ,X., Liao, H., and Ma, Y.: A humidity-based exposure index representing
570 ozone damage effects on vegetation, *Environ. Res. Lett.*, 16, 044030,
571 <https://doi.org/10.1088/1748-9326/abecbb>, 2021.

572 Grell, G. A., McKeen, S., Michalakes, J., Bao, J.-W., Trainer, M., and Hsie, E.-Y.: Real-
573 time simultaneous prediction of air pollution and weather during the Houston 2000
574 Field Experiment, presented at the 4th Conference on Atmospheric Chemistry:

575 Atmospheric Chemistry and Texas Field Study, 13–17 January, American
576 Meteorological Society, Orlando, 2002.

577 Grell, G. A., Peckham, S. E., Schmitz, R., McKeen, S. A., Frost, G., Skamarock, W. C.,
578 and Eder, B.: Fully coupled “online” chemistry within the WRF model. *Atmos.*
579 *Environ.*, 39, 6957–6975, <https://doi.org/10.1016/j.atmosenv.2005.04.027>, 2005.

580 Guenther, A., Karl, T., Harley, P., Wiedinmyer, C., Palmer, P. I., and Geron, C.:
581 Estimates of global terrestrial isoprene emissions using MEGAN (Model of
582 Emissions of Gases and Aerosols from Nature), *Atmos. Chem. Phys.*, 6, 3181–
583 3210, <https://doi.org/10.5194/acp-6-3181-2006>, 2006.

584 Hersbach, H., Bell, B., Berrisford, P., Hirahara, S., Horányi, A., Muñoz-Sabater, J.,
585 Nicolas, J., Peubey, C., Radu, R., Schepers, D., Simmons, A., Soci, C., Abdalla,
586 S., Abellán, X., Balsamo, G., Bechtold, P., Biavati, G., Bidlot, J., Bonavita, M., De
587 Chiara, G., Dahlgren, P., Dee, D., Diamantakis, M., Dragani, R., Flemming, J.,
588 Forbes, R., Fuentes, M., Geer, A., Haimberger, L., Healy, S., Hogan, R. J., Hólm,
589 E., Janisková, M., Keeley, S., Laloyaux, P., Lopez, P., Lupu, C., Radnoti, G., de
590 Rosnay, P., Rozum, I., Vamborg, F., Villaume, S., and Thépaut, J.-N.: The ERA5
591 global reanalysis, *Q. J. Roy. Meteor. Soc.*, 146, 1999–2049, 2020.

592 Hong, S.-Y., Noh, Y., and Dudhia, J.: A new vertical diffusion package with explicit
593 treatment of entrainment processes, *Mon. Weather Rev.*, 134, 2318–2341,
594 <https://doi.org/10.1175/MWR3199.1><https://doi.org/10.1175/MWR3199.1>, 2006.

595 Hu, J., Chen, J., Ying, Q., and Zhang, H.: One-year simulation of ozone and particulate
596 matter in China using WRF/CMAQ modeling system, *Atmos. Chem. Phys.*, 16,
597 10333–10350, <https://doi.org/10.5194/acp-16-10333-2016><https://doi.org/10.5194/acp-16-10333-2016>, 2016.

598 Jin, Z., Yan, D., Zhang, Z., Li, M., Wang, T., Huang, X., Xie, M., Li S and Zhuang.:
600 Effects of elevated ozone exposure on regional meteorology and air quality in
601 China through ozone-vegetation coupling. *J. Geophys. Res.-Atmos.*, 128,
602 e2022JD038119.
603 <https://doi.org/10.1029/2022JD038119><https://doi.org/10.1029/2022JD038119>,

604 2023.

605 Li, J., Mahalov, A., and Hyde, P.: Simulating the impacts of chronic ozone exposure on
606 plant conductance and photosynthesis, and on the regional hydroclimate using
607 WRF/Chem, Environ. Res. Lett., 11, 114017,
608 <https://doi.org/10.1088/17489326/11/11/114017>, 2016.

609 Li, P., Calatayud, V., Gao, F., Uddling, J., and Feng, Z. Z.: Differences in ozone
610 sensitivity among woody species are related to leaf morphology and antioxidant
611 levels, Tree Physiol., 36, 1105– 1116, <https://doi.org/10.1093/treephys/tpw042>,
612 2016.

613 Li, P., Feng, Z., Catalayud, V., Yuan, X., Xu, Y., and Paoletti, E.: A meta-analysis on
614 growth, physiological, and biochemical responses of woody species to ground-
615 level ozone highlights the role of plant functional types, Plant Cell Environ., 40,
616 2369–2380, <https://doi.org/10.1111/pce.13043>, 2017.

617 Liu, Y. and Wang, T.: Worsening urban ozone pollution in China from 2013 to 2017 –
618 Part 1: The complex and varying roles of meteorology, Atmos. Chem. Phys., 20,
619 6305–6321, <https://doi.org/10.5194/acp-20-6305-2020>, 2020.

620 Lombardozzi, D., Levis, S., Bonan, G., and Sparks, J. P.: Predicting photosynthesis and
621 transpiration responses to ozone: decoupling modeled photosynthesis and stomatal
622 conductance, Biogeosciences, 9, 3113–3130, <https://doi.org/10.5194/bg-9-31132012>, 2012.

624 Lombardozzi, D., Sparks, J. P., and Bonan, G.: Integrating O₃ influences on terrestrial
625 processes: photosynthetic and stomatal response data available for regional and
626 global modeling, Biogeosciences, 10, 6815–6831, <https://doi:10.5194/bg-10-6815-2013>, 2013.

628 Lombardozzi, D., Levis, S., Bonan, G., Hess, P. G., and Sparks, J. P.: The influence of
629 chronic ozone exposure on global carbon and water cycles, J. Climate, 28, 292–
630 305, <https://doi.org/10.1175/JCLI-D-14-00223.1>, 2015.

631 Matyssek, R., Sandermann, H., Wieser, G., Booker, F., Cieslik, S., Musselman, R., and
632 Ernst, D.: The challenge of making ozone risk assessment for forest trees more

633 mechanistic, Environ. Pollut., 156, 567–582,
634 <https://doi:10.1016/j.envpol.2008.04.017>, 2008.

635 Mlawer, E. J., Taubman, S. J., Brown, P. D., Iacono, M. J., and Clough, S. A.: Radiative
636 transfer for inhomogeneous atmosphere: RRTM, a validated correlated-k model
637 for the longwave, *J. Geophys. Res-Atmos.*, 102(D14), 16 663–16 682,
638 <https://doi.org/10.1029/97JD00237> <https://doi.org/10.1029/97JD00237>, 1997.

639 Monks, P. S., Archibald, A. T., Colette, A., Cooper, O., Coyle, M., Derwent, R., Fowler,
640 D., Granier, C., Law, K. S., Mills, G. E., Stevenson, D. S., Tarasova, O., Thouret,
641 V., von Schneidemesser, E., Sommariva, R., Wild, O., and Williams, M. L.:
642 Tropospheric ozone and its precursors from the urban to the global scale from air
643 quality to short-lived climate forcer, *Atmos. Chem. Phys.*, 15, 8889–8973,
644 <https://doi.org/10.5194/acp-15-8889-2015>, 2015.

645 Morrison, H., Thompson, G., and Tatarki, V.: Impact of cloud microphysics on the
646 development of trailing stratiform precipitation in a simulated squall line:
647 comparison of one- and two-moment schemes, *Monthly Weather Review*, 137,
648 991–1007, <https://doi.org/10.1175/2008MWR2556.1>, 2009.

649 Niu, G. Y., Yang, Z. L., Mitchell, K. E., Chen, F., Ek, M. B., Barlage, M., Kumar, A.,
650 Manning, K., Niyogi, D., Rosero, E., Tewari, M., and Xia, Y.: The community
651 Noah land surface model with multiparameterization options (Noah-MP): 1.
652 Model description and evaluation with local-scale measurements, *J. Geophys.
653 Res-Atmos.*, 116, D12, <https://doi.org/10.1029/2010JD015139>, 2011.

654 Ren, W., Tian, H., Tao, B., Chappelka, A., Sun, G., Lu, C., Liu, M., Chen, G., and Xu,
655 X.: Impacts of tropospheric ozone and climate change on net primary productivity
656 and net carbon exchange of China's forest ecosystems, *Glob. Ecol. Biogeogr.*, 20,
657 391–406, <https://doi.org/10.1111/j.1466-8238.2010.00606.x>, 2011.

658 Sadiq, M., Tai, A. P. K., Lombardozzi, D., and Val Martin, M.: Effects of ozone–
659 vegetation coupling on surface ozone air quality via biogeochemical and
660 meteorological feedbacks, *Atmos. Chem. Phys.*, 17, 3055–3066,
661 <https://doi.org/10.5194/acp-17-3055-2017>, 2017.

662 Sitch, S., Cox, P. M., Collins, W. J., and Huntingford, C.: Indirect radiative forcing of
663 climate change through ozone effects on the land-carbon sink, *Nature*, 448, 791–
664 794, <https://doi.org/10.1038/nature06059>, 2007.

665 Skamarock W C and Klemp J B. A time-split nonhydrostatic atmospheric model for
666 weather research and forecasting applications. *J. Comput. Phys.*, 227(7): 3465-
667 3485,
668 <https://doi.org/10.1016/j.jcp.2007.01.037>
669 <https://doi.org/10.1016/j.jcp.2007.01.037>, 2008.

670 Su, B., Zhou, M., Xu, H., Zhang, X., Li, Y., Su, H., and Xiang B.: Photosynthesis
671 and biochemical responses to elevated O₃ in *Plantago major* and *Sonchus*
672 *oleraceus* growing in a lowland habitat of northern China, *J. Environ. SCI.*, 53(3):
673 113-121,
674 <https://doi.org/10.1016/j.jes.2016.05.011>
675 <https://doi.org/10.1016/j.jes.2016.05.011>, 2017.

676 Tie, X. X., Madronich, S., Walters, S., Zhang, R. Y., Rasch, P., and Collins, W.: Effect
677 of clouds on photolysis and oxidants in the troposphere, *J. Geophys. Res.-Atmos.*,
678 108, 4642,
679 <https://doi.org/10.1029/2003jd003659>
680 <https://doi.org/10.1029/2003jd003659>, 2003.

681 Wan, W., Manning, WJ., Wang, X., Zhang, H., Sun, X., and Zhang, Q.: Ozone and
682 ozone injury on plants in and around Beijing, China, *Environ Pollut.*, 191: 215-
683 222, <https://doi.org/10.1016/j.envpol.2014.02.035>, 2014

684 Wilkinson, S., Clephan, A. L., and Davies, W. J.: Rapid Low Temperature-Induced
685 Stomatal Closure Occurs in Cold-Tolerant *Commelina Communis* Leaves But Not
686 in Cold-Sensitive Tobacco Leaves, via a Mechanism That Involves Apoplastic
687 Calcium But Not Abscisic Acid. *Plant Physiol.*, 126, 1566–1578.
688 <https://doi.org/10.1104/pp.126.4.1566>, 2001.

689 Wittig, V. E., Ainsworth, E. A., and Long, S. P.: To what extent do current and projected
690 increases in surface ozone affect photosynthesis and stomatal conductance of trees?

691 A metaanalytic review of the last 3 decades of experiments, *Plant Cell Environ.*,
692 30, 1150–1162, <https://doi.org/10.1111/j.13653040.2007.01717.x>, 2007.

693 Xie, X., Wang, T., Yue, X., Li, S., Zhuang, B., Wang, M., and Yang, X.: Numerical
694 modeling of ozone damage to plants and its effects on atmospheric CO₂ in China,
695 *Atmos. Environ.*, 217, 116970, <https://doi.org/10.1016/j.atmosenv.2019.116970>,
696 2019.

697 Yue, X. and Unger, N.: Ozone vegetation damage effects on gross primary productivity
698 in the United States, *Atmos. Chem. Phys.*, 14, 9137–9153,
699 <https://doi.org/10.5194/acp-14-9137-2014>, 2014.

700 Yue, X. and Unger, N.: The Yale Interactive terrestrial Biosphere model version 1.0:
701 description, evaluation and implementation into NASA GISS ModelE2, *Geosci.*
702 *Model Dev.*, 8, 2399–2417, <https://doi.org/10.5194/gmd-8-2399-2015>, 2015.

703 Zaveri, R. A., and Peters, L. K.: A new lumped structure photochemical mechanism for
704 large-scale applications, *J Geophys Res-Atmos.*, 104, 30387-30415, 1999.

705 Zaveri, R. A., Easter, R. C., Fast, J. D., and Peters, L. K.: Model for simulating aerosol
706 interactions and chemistry (MOSAIC), *J. Geophys. Res-Atmos.*, 113, D13204,
707 <https://doi.org/10.1029/2007JD008782>, 2008.

708 Zhou, S. S., Tai, A. P. K., Sun, S., Sadiq, M., Heald, C. L., and Geddes, J. A.: Coupling
709 between surface ozone and leaf area index in a chemical transport model: strength
710 of feedback and implications for ozone air quality and vegetation health, *Atmos.*
711 *Chem. Phys.*, 18, 14133–14148, <https://doi.org/10.5194/acp-18-14133-2018>, 2018.

712 Zhu, J., Tai, A. P. K., and Yim, S. H. L.: Effects of ozone-vegetation interactions on
713 meteorology and air quality in China using a two-way coupled land-atmosphere
714 model, *Atmos. Chem. Phys.*, 22, 765-782, <https://doi.org/10.5194/acp-22-765-2022>, 2022.

715

716

717 **Tables**718 **Table 1.** Parameters used for S2007 O₃ damage scheme.

| PFTs ^a | a_{PFT} (nmol ⁻¹ m ² s) ^b | y_{PFT} (nmol m ⁻² s ⁻¹) |
|-------------------|--|---|
| EBF | 0.075, 0.02 | 1.6 |
| NF | 0.075, 0.02 | 1.6 |
| DBF | 0.15, 0.04 | 1.6 |
| SHR | 0.1, 0.03 | 1.6 |
| GRA | 1.4, 0.25 | 5 |
| CRO | 1.4, 0.25 | 5 |

719 ^a The plant functional types (PFTs) include evergreen broadleaf forest (EBF), needleleaf
 720 forest (NF), deciduous broadleaf forest (DBF), shrubland (SHR), grassland (GRA), and
 721 cropland (CRO).

722 ^b The first number is for high sensitivity and the second is for low sensitivity.

723

724

725

Table 2. Slopes and intercepts used for L2013 O₃ damage scheme.

| PFTs | a_p (mmol m ⁻²) | b_p | a_c (mmol m ⁻²) | b_c |
|------|-------------------------------|--------|-------------------------------|--------|
| EBF | 0 | 0.8752 | 0 | 0.9125 |
| NF | 0 | 0.839 | 0.0048 | 0.7823 |
| DBF | 0 | 0.8752 | 0 | 0.9125 |
| SHR | 0 | 0.8752 | 0 | 0.9125 |
| GRA | -0.0009 | 0.8021 | 0 | 0.7511 |
| CRO | -0.0009 | 0.8021 | 0 | 0.7511 |

726

727

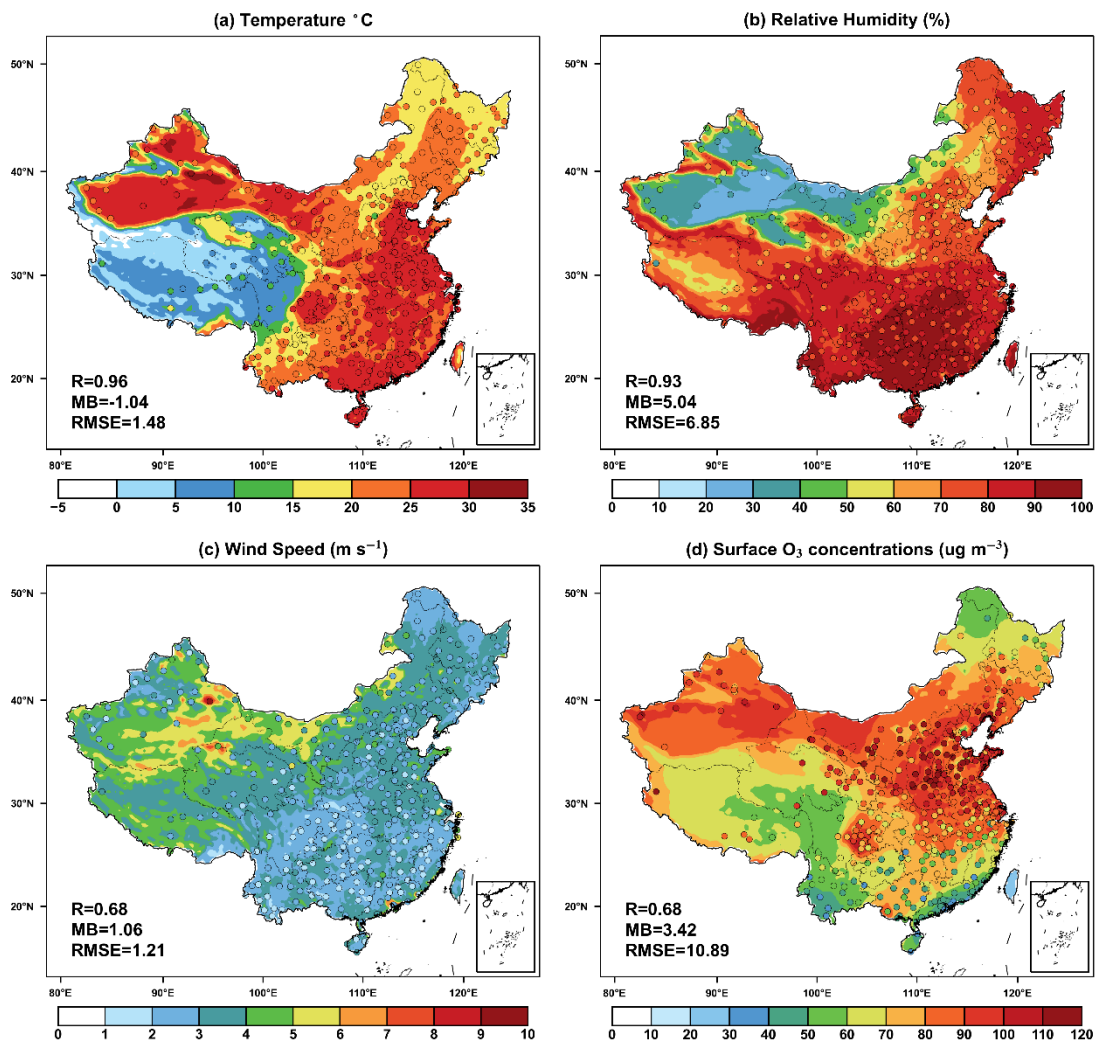
728

Table 3. Summary of simulation experiments

| Name | O ₃ damage to vegetable | Scheme |
|--------------|---------------------------------------|---------------------------|
| CRTL | - | - |
| Offline_SH07 | High | Sitch et al. (2007) |
| Offline_SL07 | Low | Sitch et al. (2007) |
| Offline_L13 | - | Lombardozzi et al. (2013) |
| Online_SH07 | High | Sitch et al. (2007) |
| Online_SL07 | Low | Sitch et al. (2007) |
| Online_L13 | - | Lombardozzi et al. (2013) |

732

Figure captions

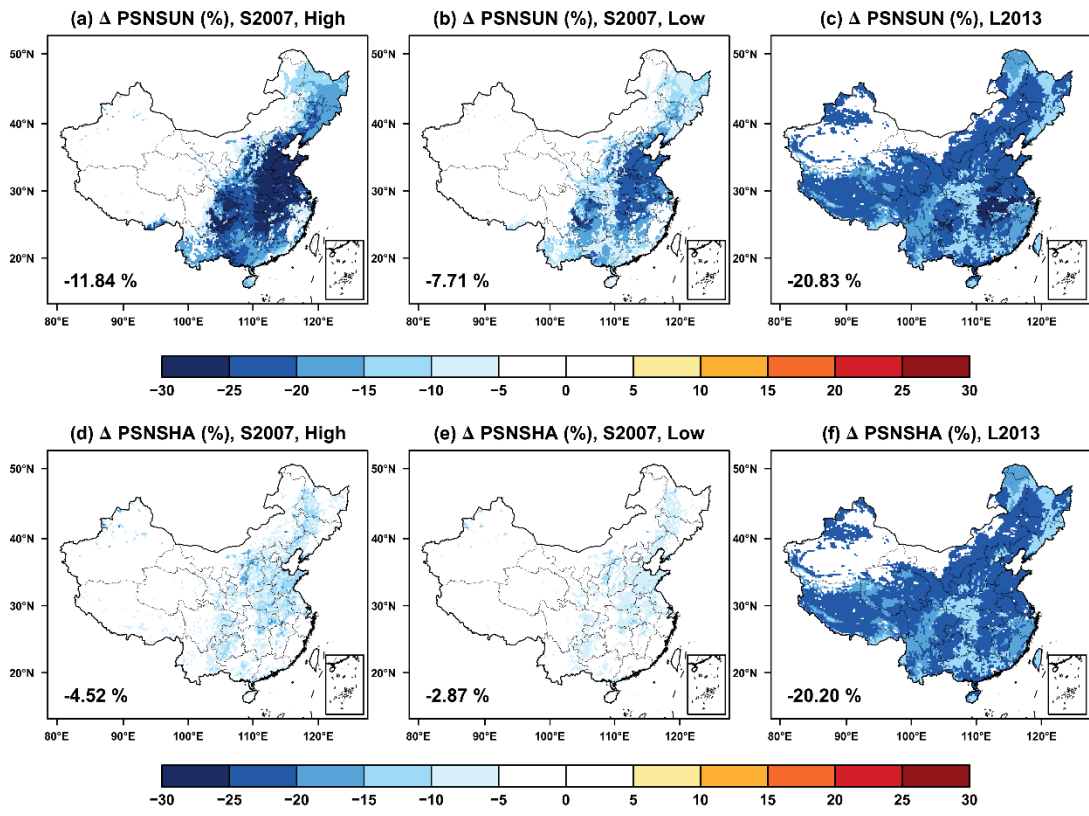


733

734

735

736 **Figure 1** Evaluations of simulated summer (June–August) daily (24-h average) (a)
 737 near-surface temperature, (b) relative humidity, (c) wind speed, and (d) surface O₃
 738 concentrations in China. The dots represent the site-level observations. The correlation
 739 coefficients (R), mean biases (MB), and root-mean-square error (RMSE) for the
 740 comparisons are shown in the lower left corner of each panel.
 741

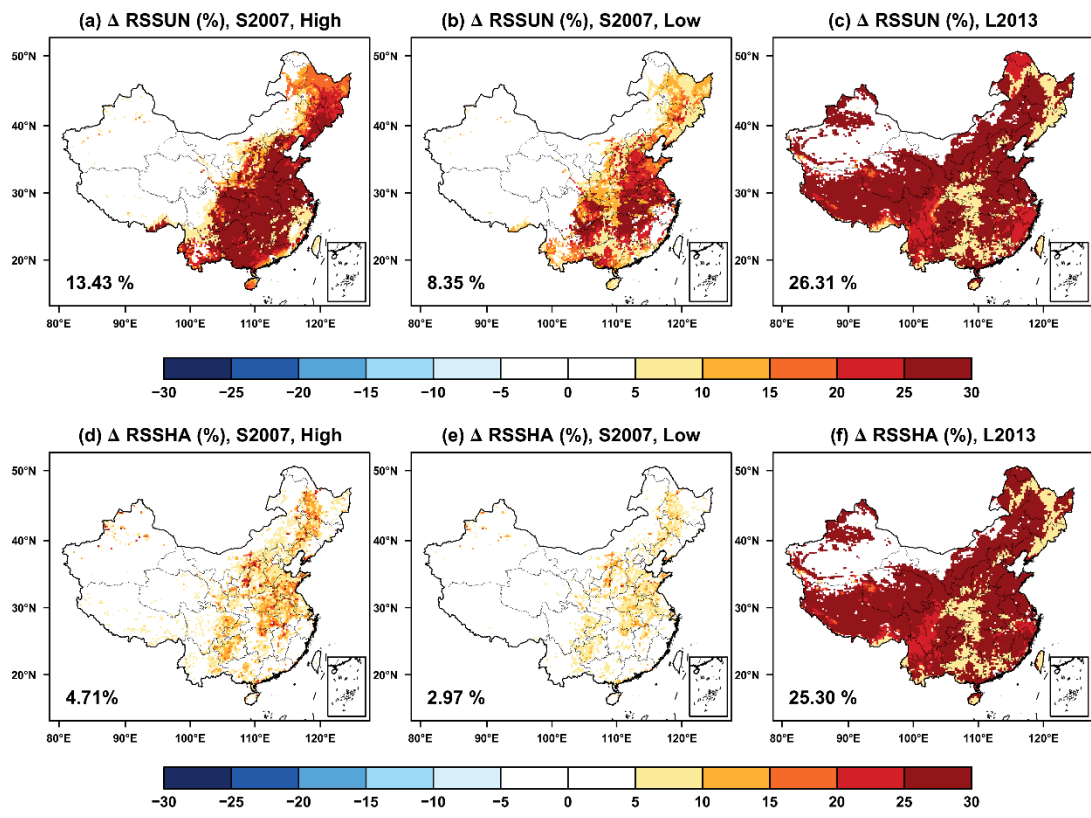


742

743

744 **Figure 2** Offline O₃ damage (%) to the summertime photosynthesis of (a-c) sunlit and
 745 (d-f) shaded leaves predicted by the S2007 scheme with (a, d) high and (b, e) low
 746 sensitivities or the (c, f) L2013 scheme. The area-weighted percentage changes are
 747 shown in the lower left corner.

748

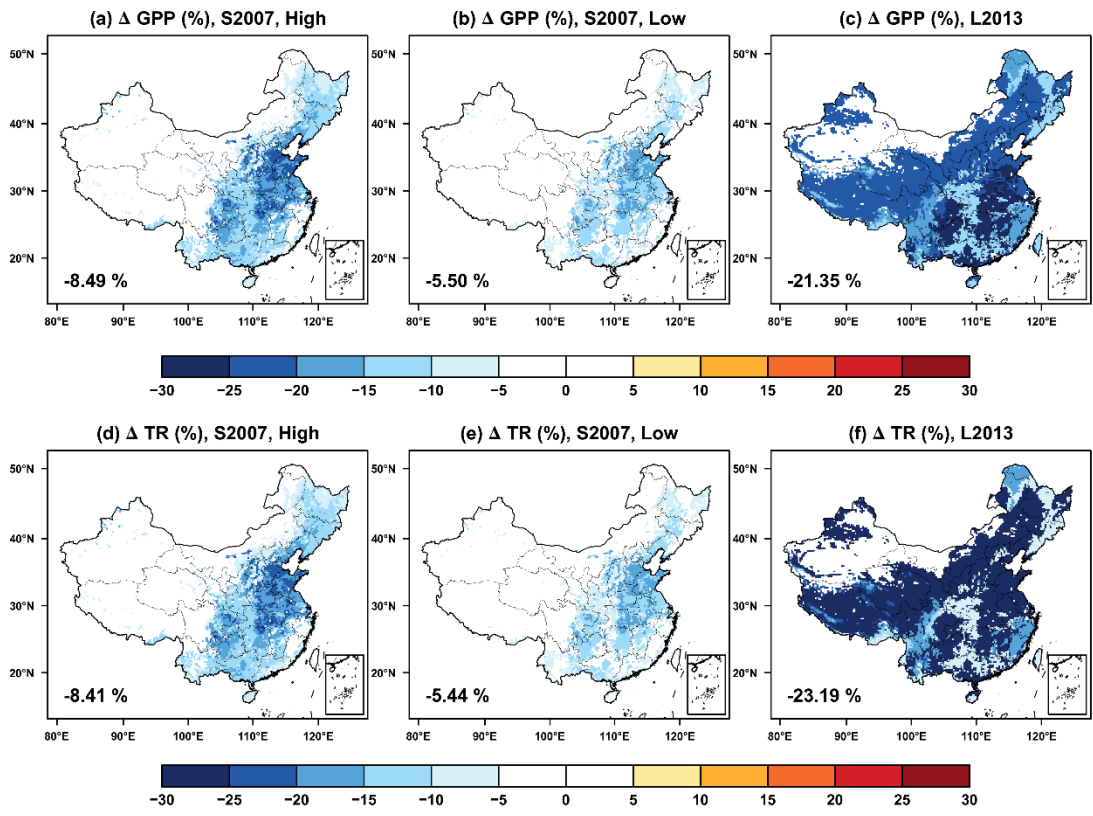


749

750

751 **Figure 3** The same as Figure 2 but for the changes in stomatal resistance.

752

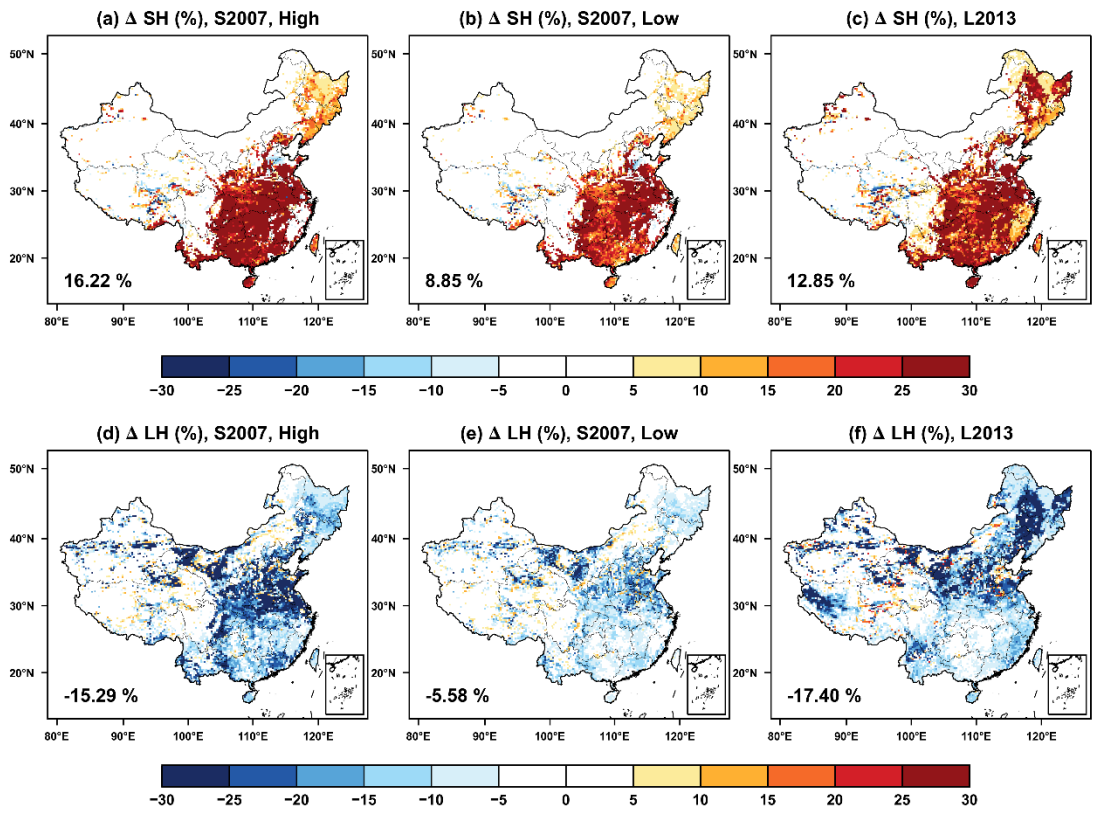


753

754

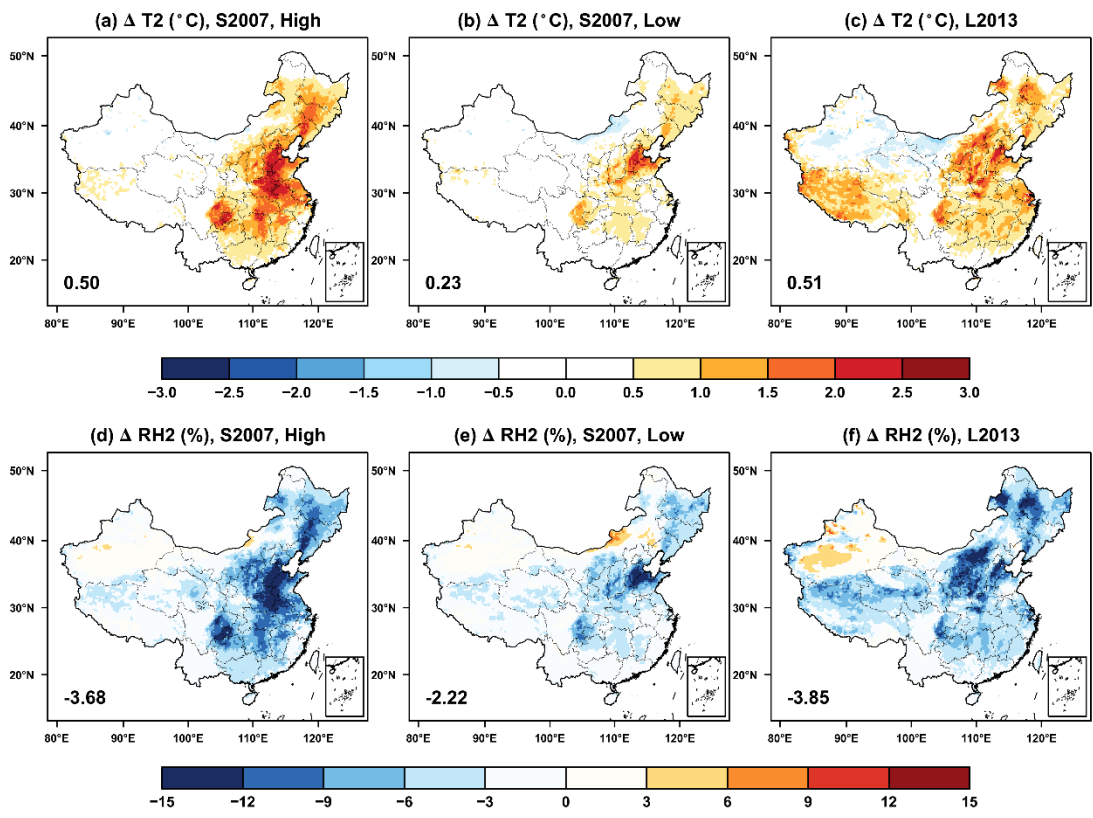
755 **Figure 4** Offline O₃ damage (%) to the (a-c) gross primary productivity (GPP) and (d-f) transpiration rate (TR) predicted by the Sitch scheme with (a, d) high and (b,e) low
756 sensitivities or the (c, f) Lombardozzi scheme. The area-weighted percentage changes
757 are shown in the lower left corner.
758

759



760
761
762
763
764
765
766
767

Figure 5 The feedback of O_3 -vegetation interaction to surface (a-c) sensible and (d-f) latent heat fluxes in the summer predicted by the S2007 scheme with (a, d) high and (b, e) low sensitivities or the (c, f) L2013 scheme. The relative changes are shown with area-weighted percentage changes indicated at the lower left corner.



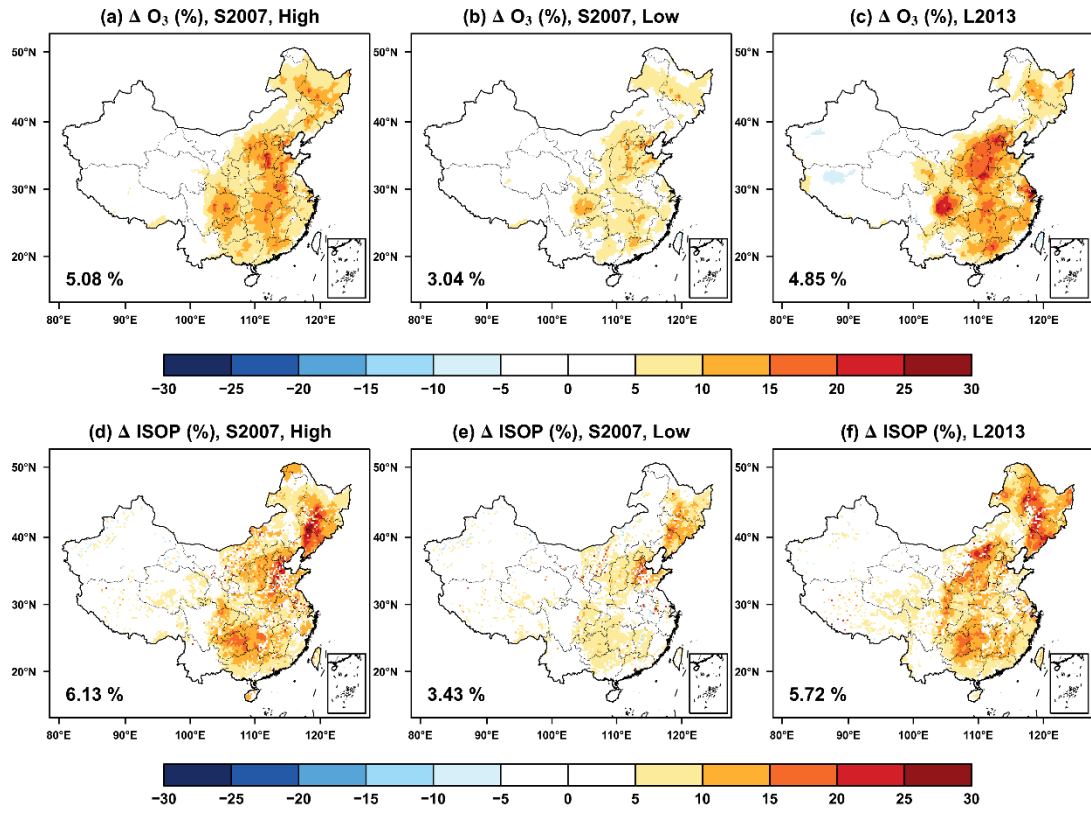
768

769

770 **Figure 6** The same as Figure 5 but for changes in (top) air temperature and (bottom)
771 relative humidity at 2 meters.

772

773



777 **Figure 7** The feedback of O₃-vegetation interaction to surface O₃ concentrations and
 778 isoprene emissions in the summer predicted by the S2007 scheme with (a, d) high and
 779 (b, e) low sensitivities or the (c, f) L2013 scheme. The area-weighted percentage
 780 changes are shown in the lower left corner.